Electronic Supplementary Material (ESI) for Journal of Materials Chemistry A.

Supporting Information

A unique 2.1 V “water in salt” elemental sulfur based Na-ion hybrid storage capacitor

Mukesh Kumar and Tharamani C. Nagaiah*

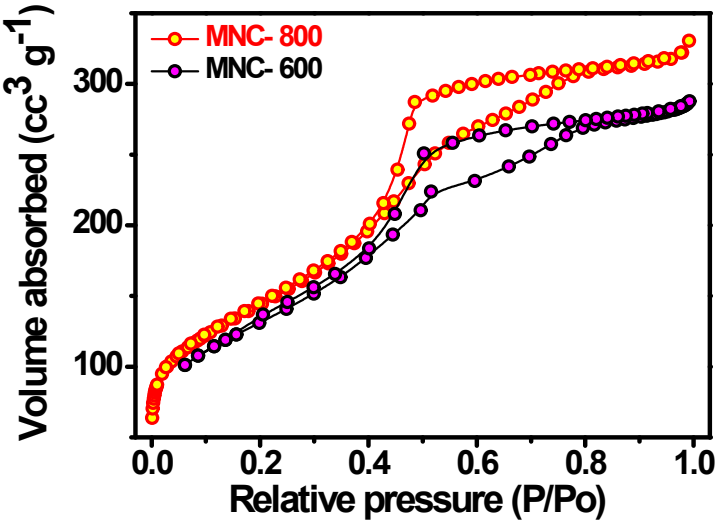

Fig. S1. Nitrogen physisorption isotherms of the MNC-600 and MNC-800 catalyst.

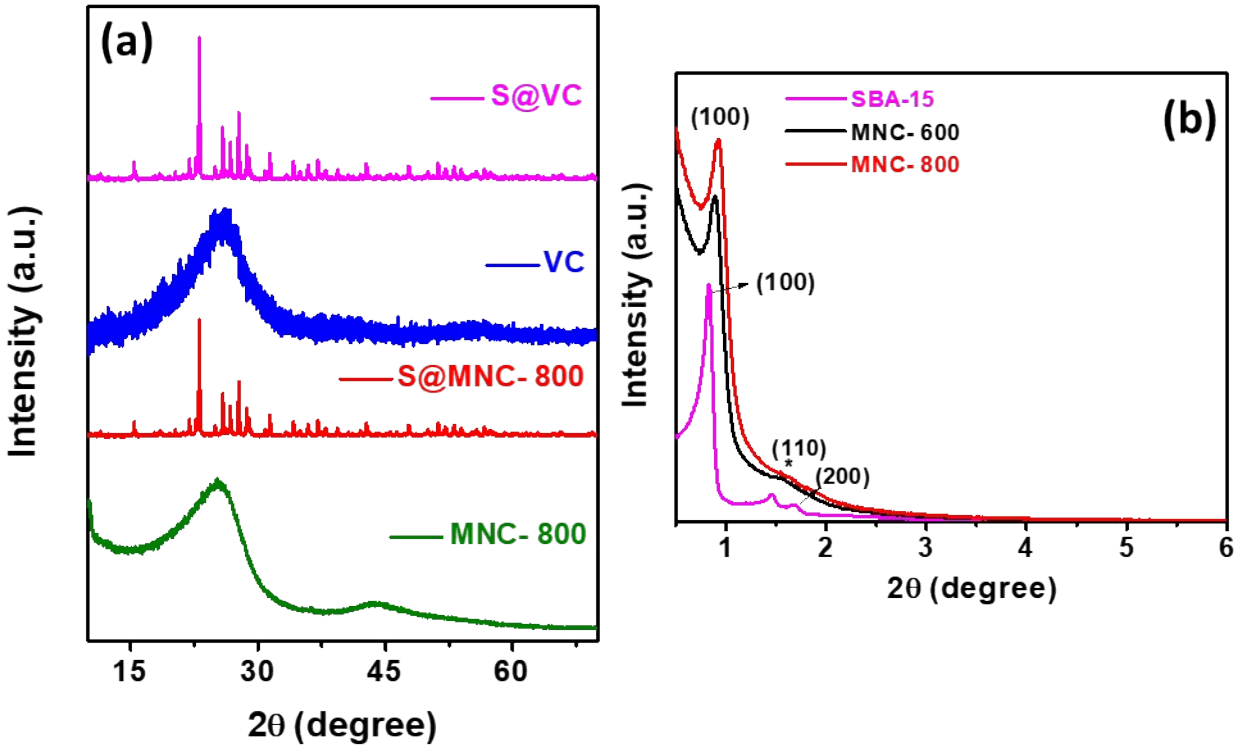

Fig. S2. (a) XRD pattern of VC and MNC-800 before and after incorporating S and (b) small angle XRD pattern of SBA-15, MNC-600, and MNC-800.

Thermogravimetric analysis (TGA):

The thermogravimetric analysis (TGA) was performed in the N_2 atmosphere using alumina pan using "TGA/DSC1" instrument from Mettler Toledo with SDTA sensor, and data were analyzed in STAR^e software (version 12.1). Thermal stability was investigated by heating from 30 °C to 800 °C at a heating rate of 10 °C/min at 40 mL/min N_2 (99.999%) flow. Each sample was tested for at least three times, and the error limit is <2%.

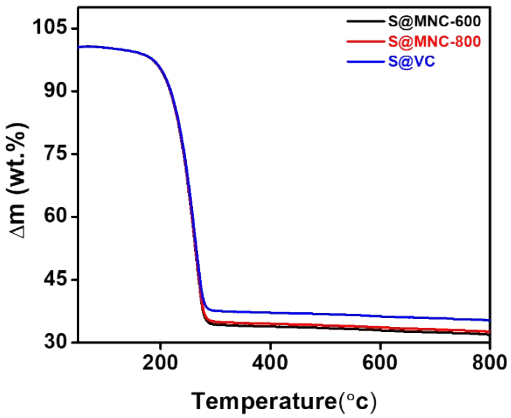

Fig. S3. (a) TGA of S@MNC-600, S@MNC-800 and S@VC.

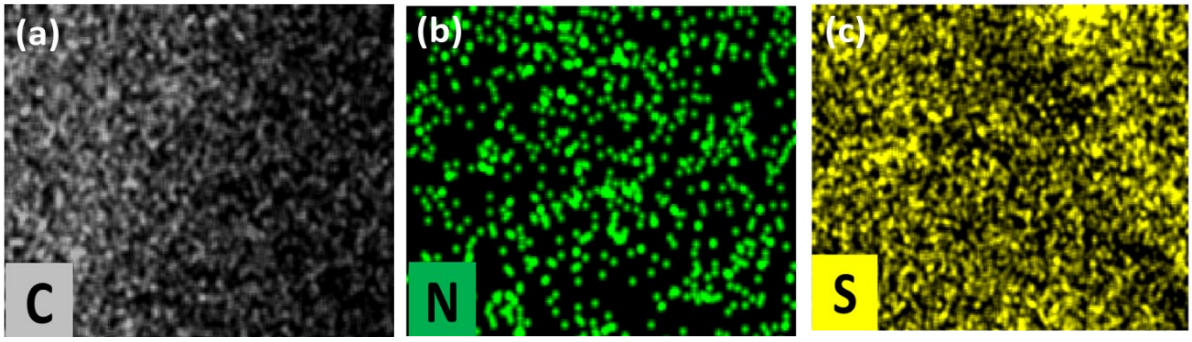

Fig. S4. elemental dot mapping images of (a) carbon, (b) nitrogen, and (c) sulfur.

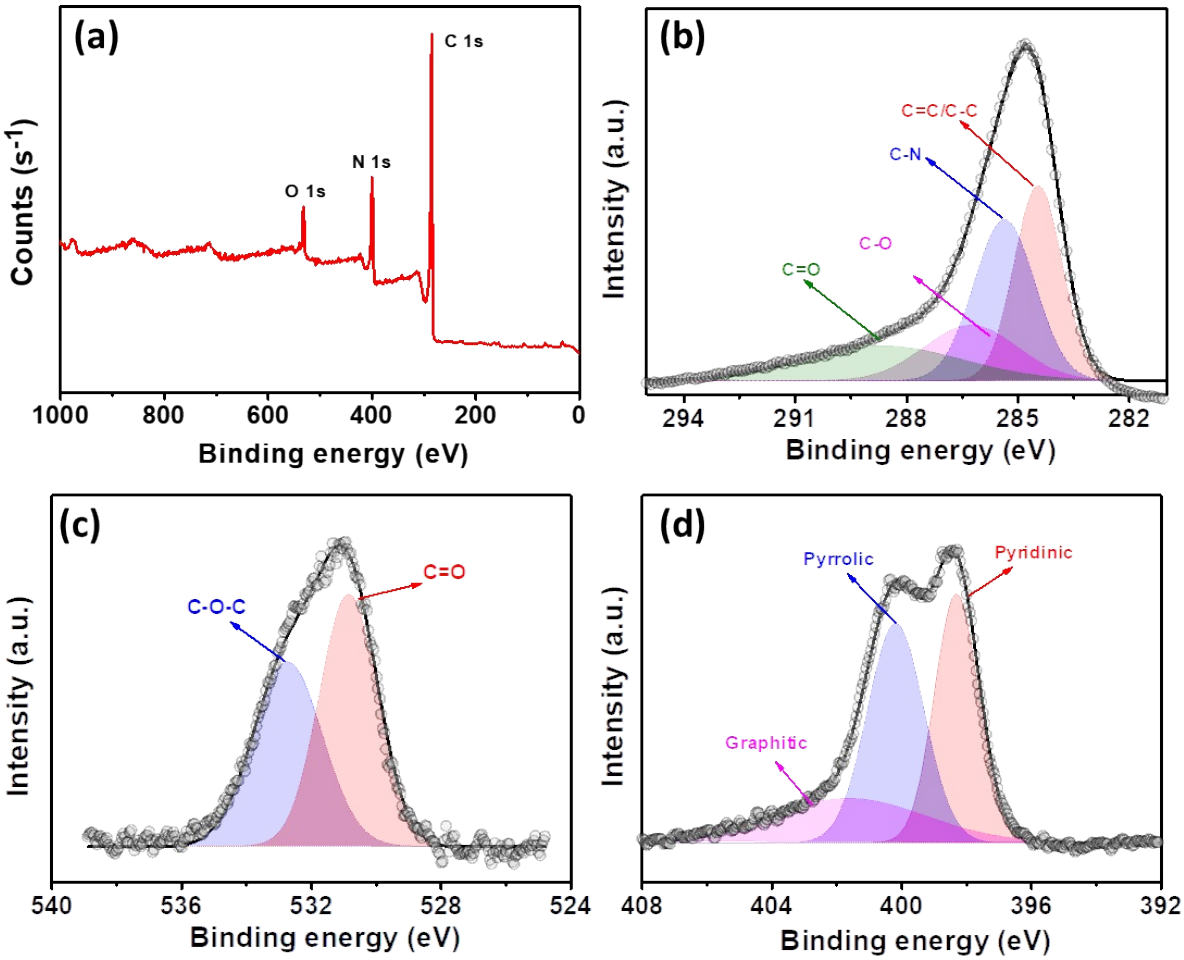

Fig. S5. (a) XPS survey spectrum and deconvoluted XP spectra of (b) C 1s, (c) O 1s, and (d) N 1s of MNC-600.

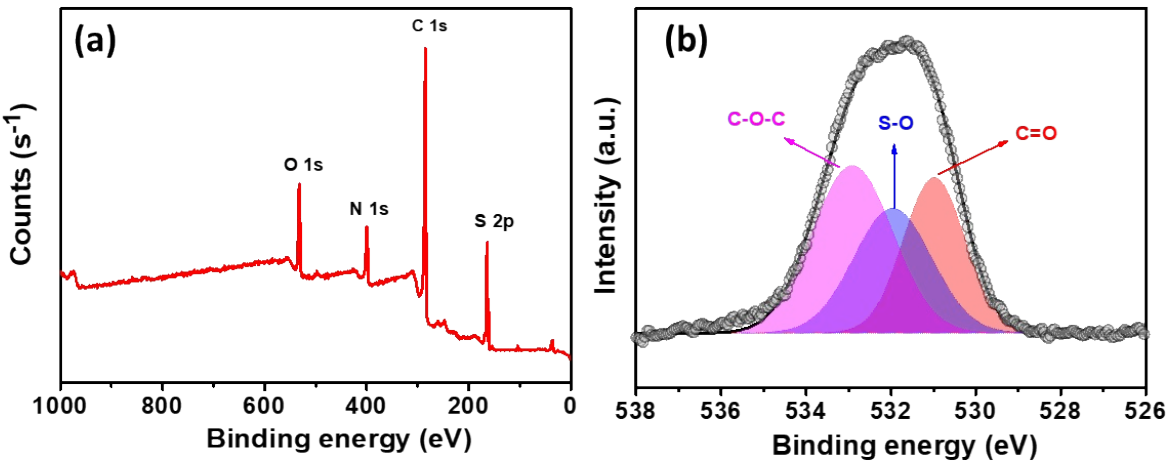

Fig. S6. (a) XPS survey spectrum and deconvoluted XP spectra of (b) O 1s, of S@MNC-600.

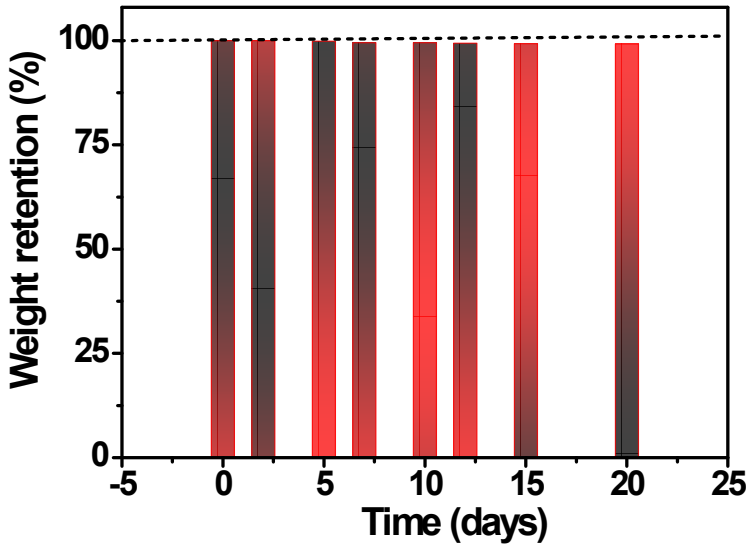

Fig. S7. Bar diagram representing the weight retention of the electrolyte at room temperature upto 20 days of analysis..

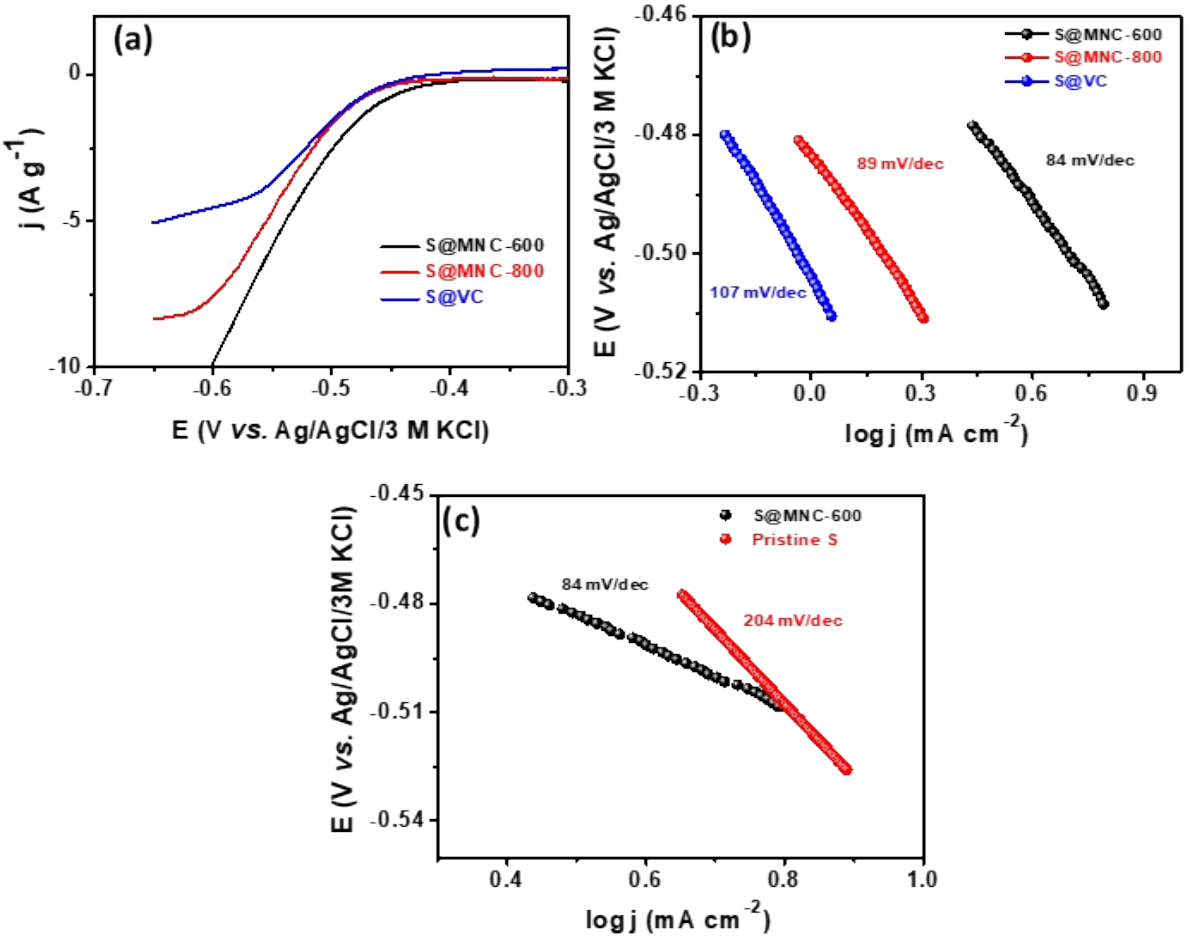

Fig. S8. Linear polarisation curve (zoomed part of CV fig. 2 a) representing the onset potential, (b) and (c) are the corresponding Tafel plot for reduction of elemental sulfur to sodium polysulfide CE: Pt wire, RE: Ag/AgCl/3 M KCl.

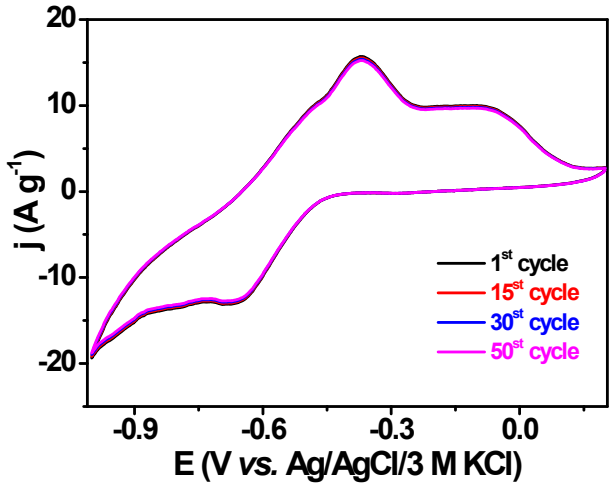

Fig. S9. Cyclic voltammograms of S@MNC-600 at 30 mV s^{-1} during stability study in 17 m aq. $NaClO_4$ electrolyte, CE: Pt wire, RE: Ag/AgCl/3 M KCl.

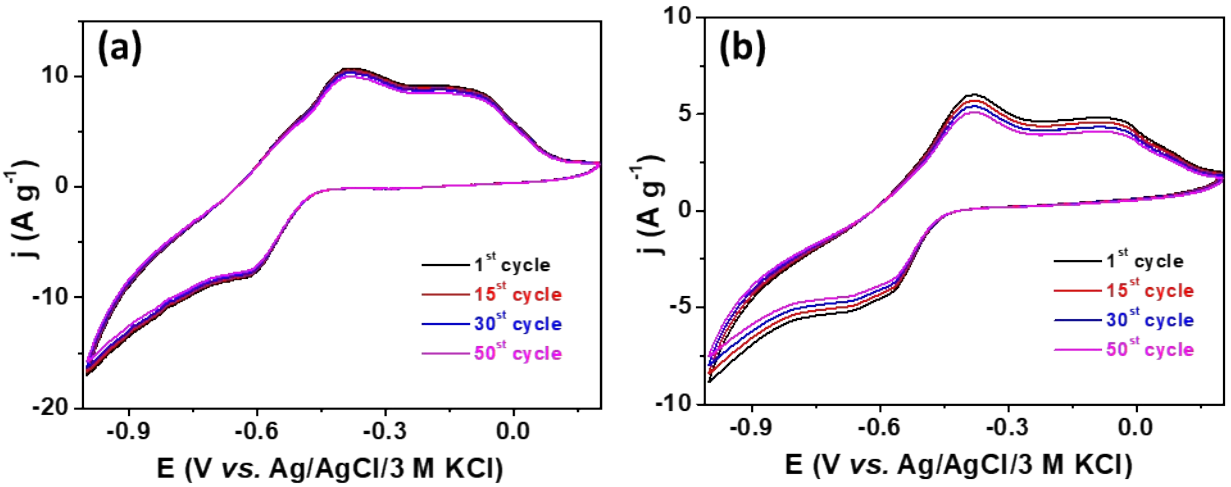

Fig. S10. Cyclic voltammograms of (a) S@MNC-800 and (b) S@VC at 30 mV s^{-1} during stability study in 17 m aq. $NaClO_4$ electrolyte, CE: Pt wire, RE: Ag/AgCl/3 M KCl.

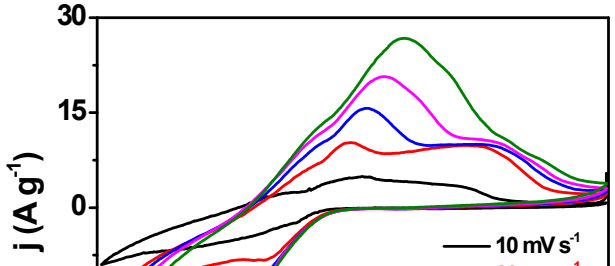

Fig. S11. Cyclic voltammograms of S@MNC-600 at various scan rates in 17 m aq. $NaClO_4$ electrolyte, CE: Pt wire, RE: Ag/AgCl/3 M KCl.

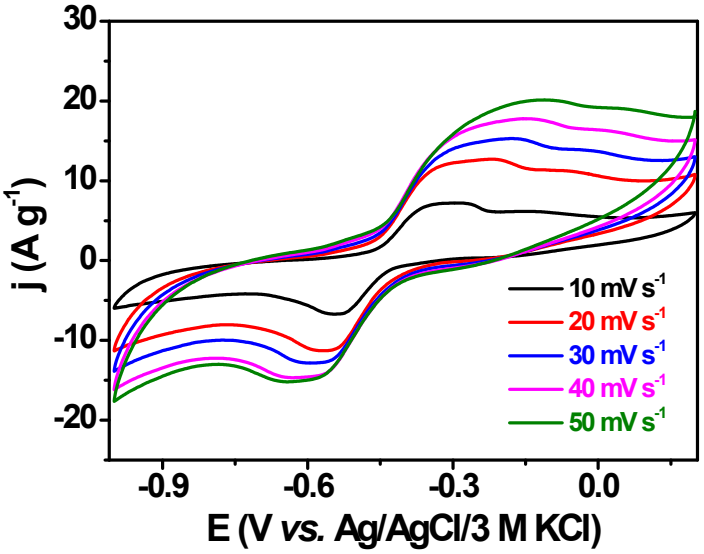

Fig. S12. Cyclic voltammograms of S@MNC-600 at various scan rates in 1 m aq. $NaClO_4$ electrolyte, CE: Pt wire, RE: Ag/AgCl/3 M KCl

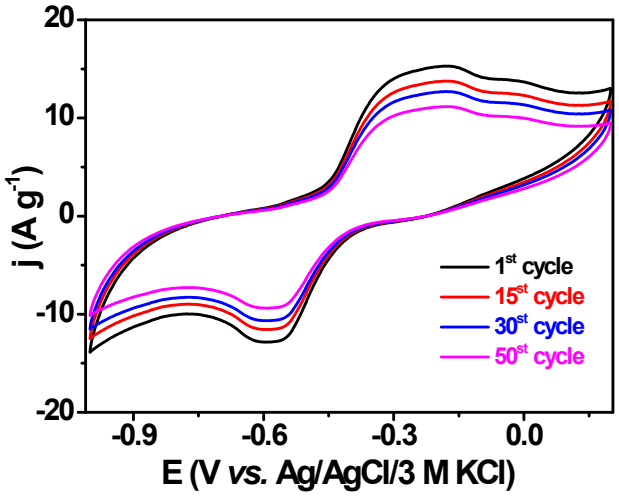

Fig. S13. Cyclic voltammograms of S@MNC-600 at 30 mV s^{-1} during stability study in 1 m aq. $NaClO_4$ electrolyte, CE: Pt wire, RE: Ag/AgCl/3 M KCl.

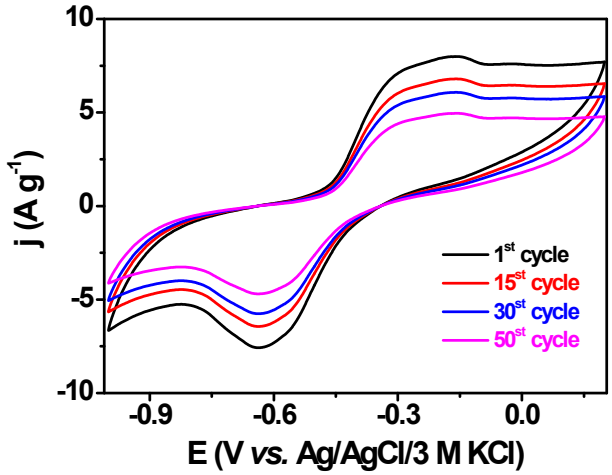

Fig. S14. Cyclic voltammograms of S@VC at 30 mV s^{-1} during stability study in 1 m aq. $NaClO_4$ electrolyte, CE: Pt wire, RE: Ag/AgCl/3 M KCl.

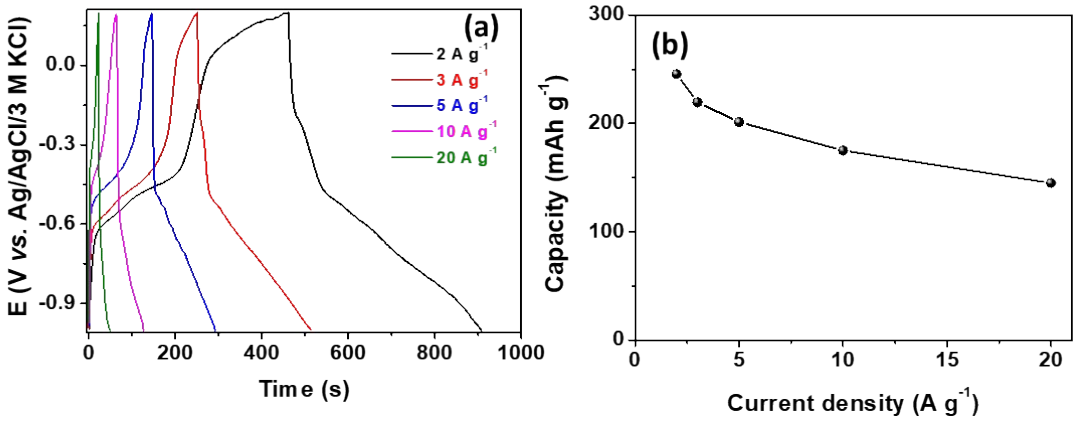

Fig. S15. GCD curves for S@MNC-800 at various current densities, and (b) corresponding capacity *vs.* current density plot in 17 m $NaClO_4$ CE: Pt wire, RE: Ag/AgCl/3 M KCl.

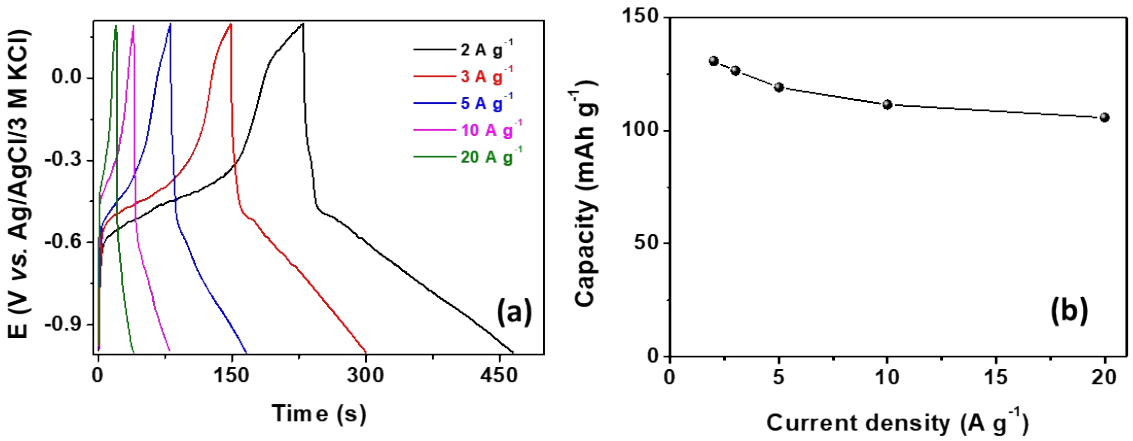

Fig. S16. GCD curves for S@VC at various current densities, (b) and (c) are the corresponding capacitance *vs.* current density and capacity *vs.* current density plot in 17 m $NaClO_4$ CE: Pt wire, RE: Ag/AgCl/3 M KCl.

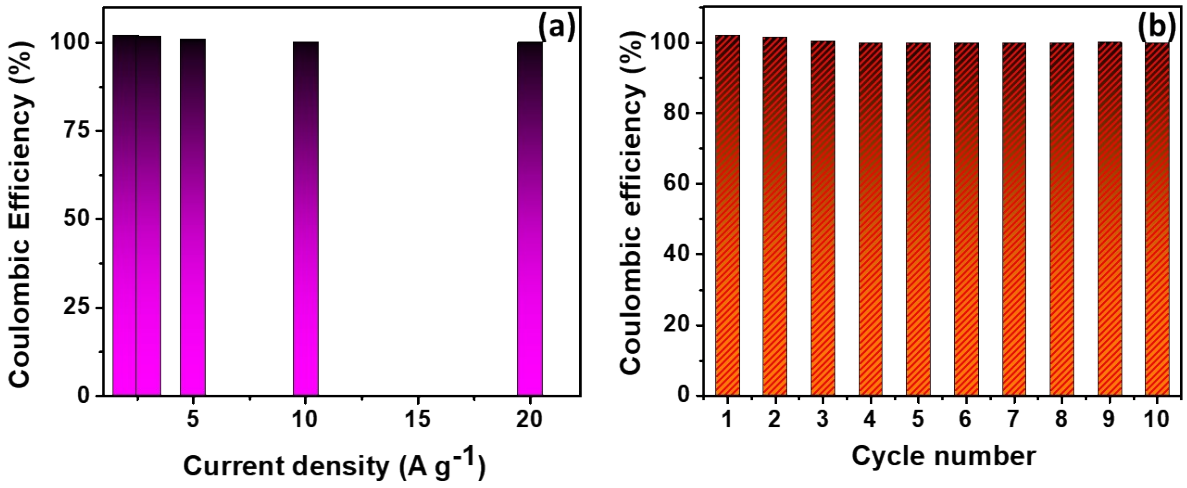

Fig. S17 Bar diagram representing the CE for S@MNC-600 negative electrode at various current densities, (b) bar diagram illustrating the CE for S@MNC-600 negative electrode at 2 A g^{-1} up to 10 consecutive cycles in 17 m $NaClO_4$.

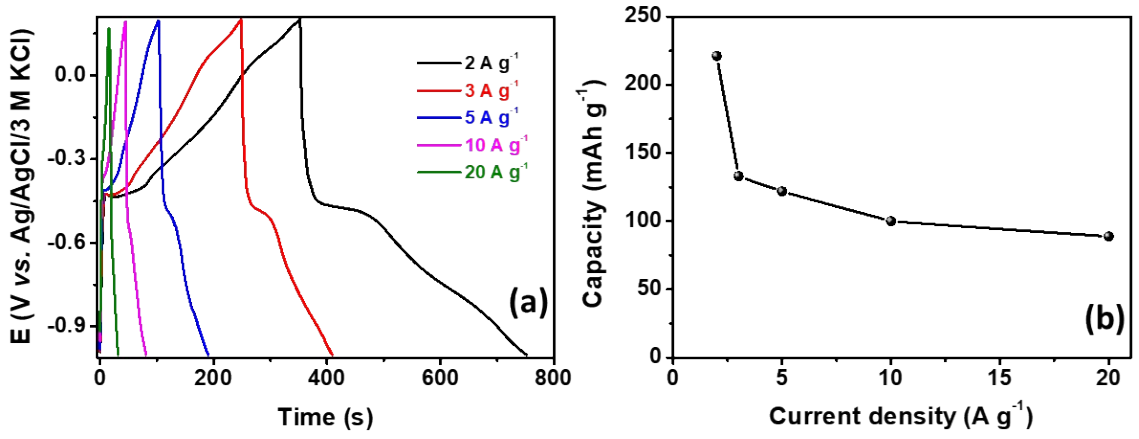

Fig. S18. GCD curves for S@MNC-600 at various current densities, (b) and (c) are the corresponding capacitance *vs.* current density and capacity *vs.* current density plot in 1 m $NaClO_4$ CE: Pt wire, RE: Ag/AgCl/3 M KCl.

Table S1: Showing the maximum solubility of various sodium salts.[1]

Salt	**Maximum conc. (m)**
NaCl	6
CH_3COONa	6
Na_2SO_4	2
$NaNO_3$	10.7
$NaClO_4$	17

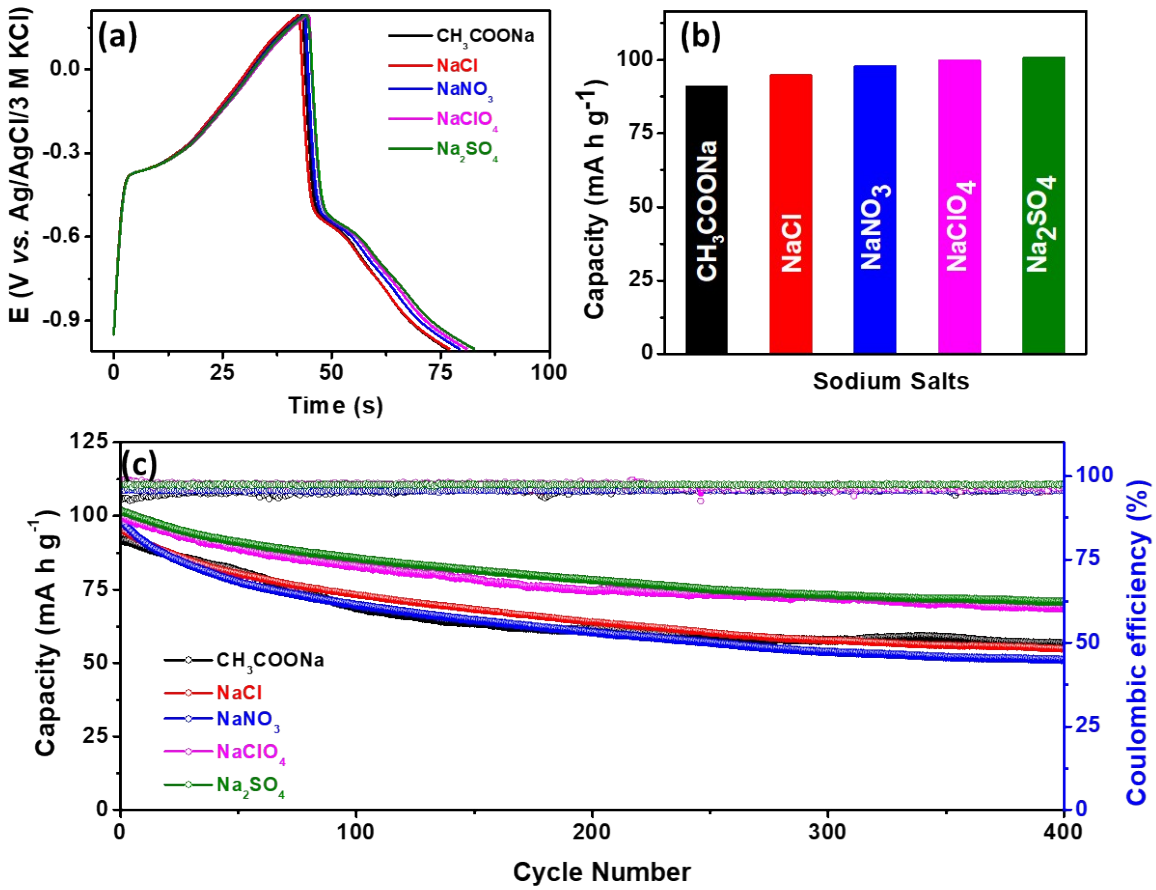

Fig. S19 (a) Charge discharge curves, (b) corresponding capacity for S@MNC-600 in various sodium salts @ 10 A g^{-1}, and (c) cycling stability of S@MNC-600 up to 400 cycles at 20 A g^{-1} in 17 m $NaClO_4$.

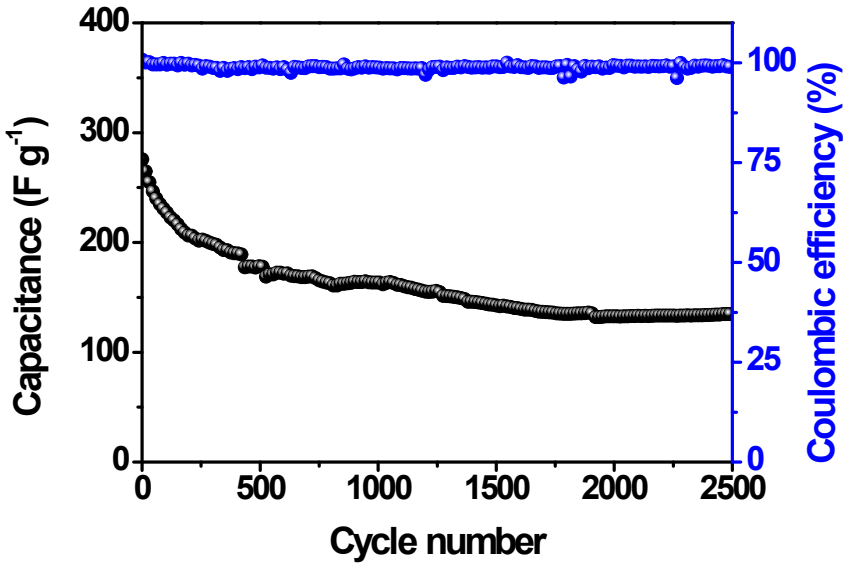

Fig. S20. Cycling stability of S@MNC-600 up to 2500 cycles at 20 A g^{-1} in 1 m $NaClO_4$ CE: Pt wire, RE: Ag/AgCl/3 M KCl.

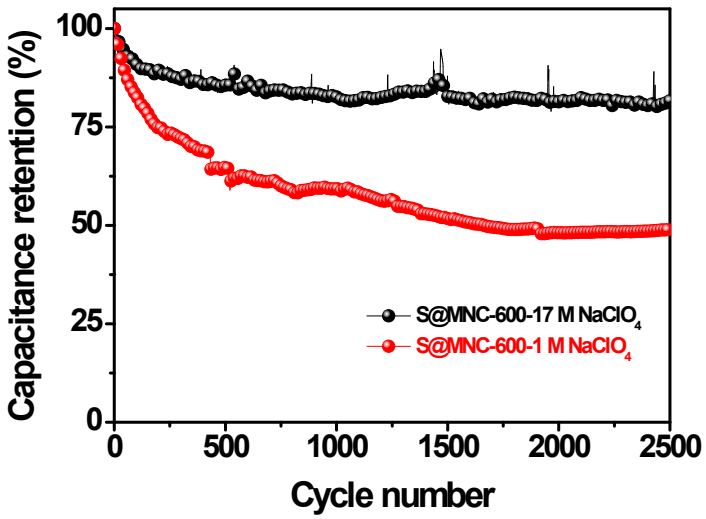

Fig. S21. Comparisons of capacitance retention of S@MNC-600 in 1 m and 17 m $NaClO_4$ over 2500 cycles at 20 A g^{-1} CE: Pt wire, RE: Ag/AgCl/3 M KCl.

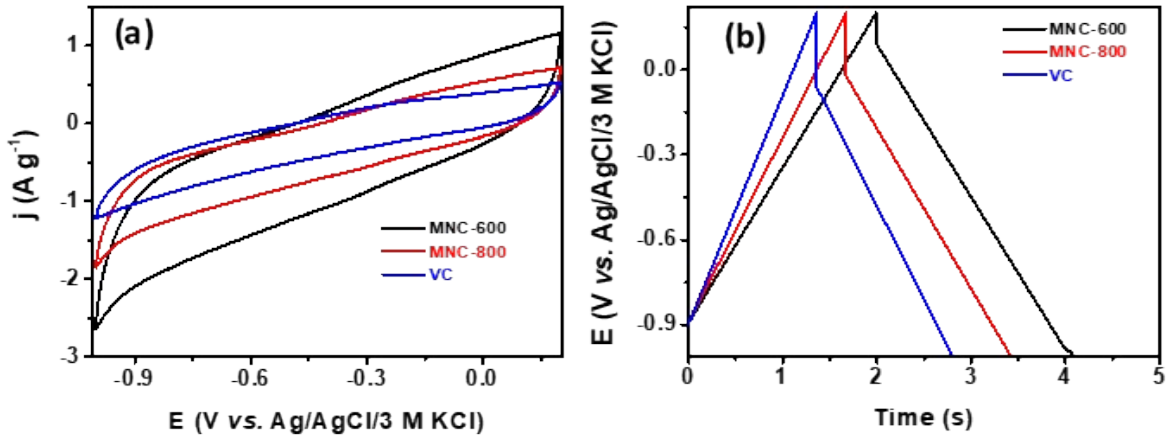

Fig. S22. (a) CVs at a scan rate of 30 mV s^{-1}, and (b) corresponding GCD curves of various catalysts at 10 A g^{-1} in 17 m $NaClO_4$ CE: Pt wire, RE: Ag/AgCl/3 M KCl.

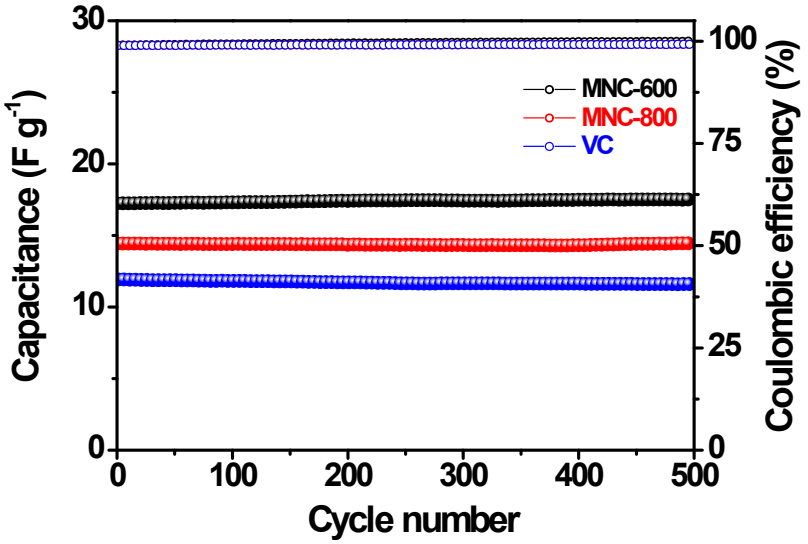

Fig. S23. Cycling stability of MNC-600, MNC-800, and VC up to 500 cycles at 10 A g^{-1} in 17 m $NaClO_4$.CE: Pt wire, RE: Ag/AgCl/3 M KCl.

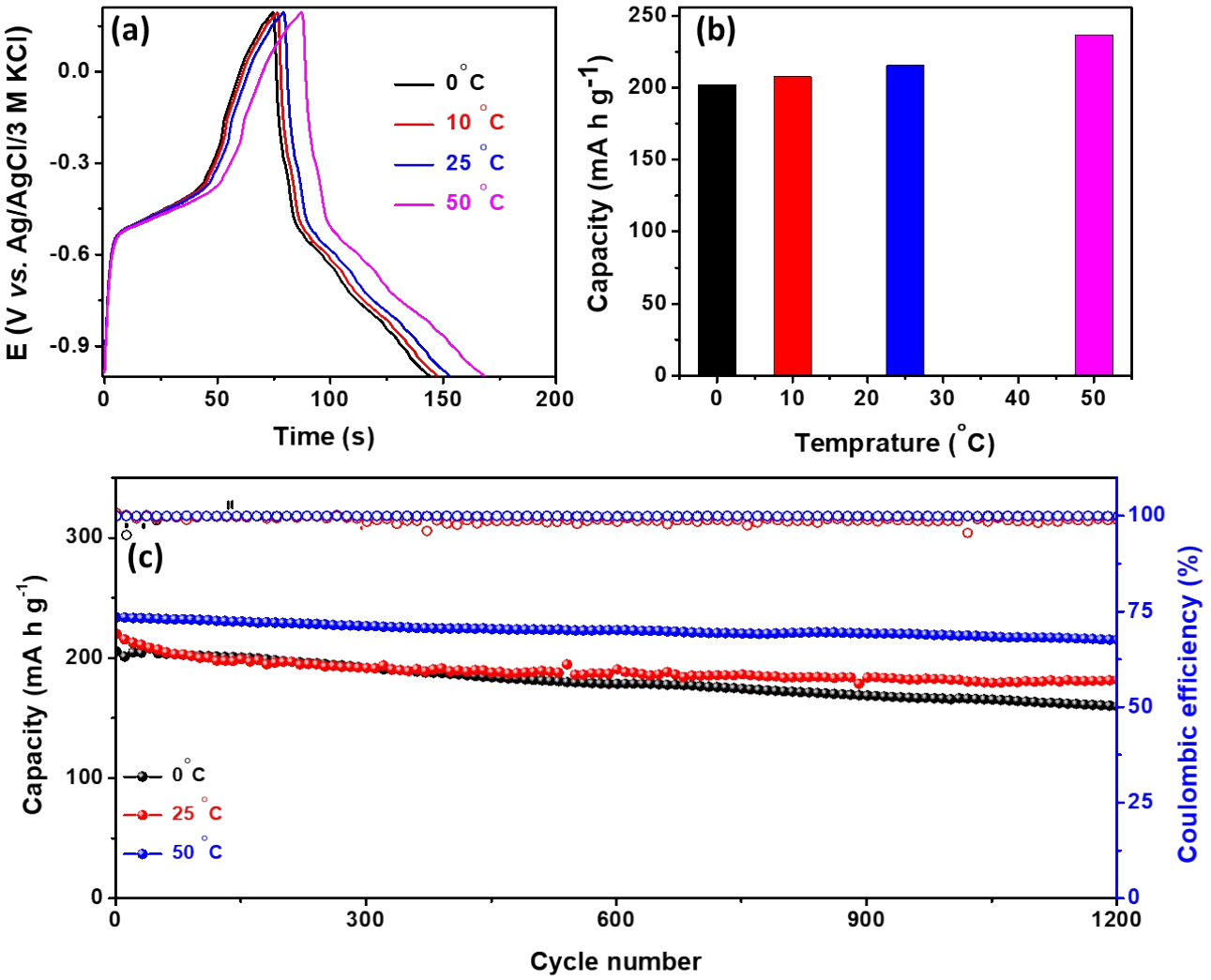

Fig. S24 (a) Charge discharge curves, (b) corresponding capacity for S@MNC-600 at various temperatures at 10 A g^{-1}, and (c) cycling stability of S@MNC-600 up to 1200 cycles at 20 A g^{-1} in 17 m $NaClO_4$.

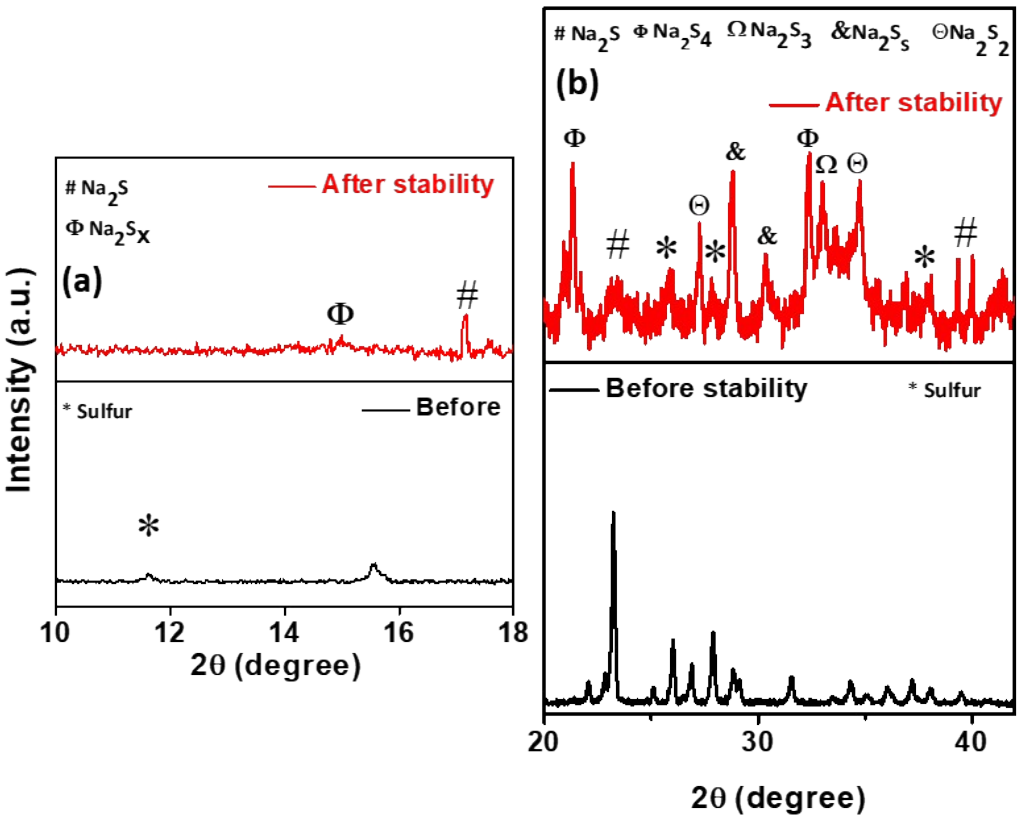

Fig. S25 XRD pattern of S@MNC-600 before and after the stability study in 17 m $NaClO_4$.

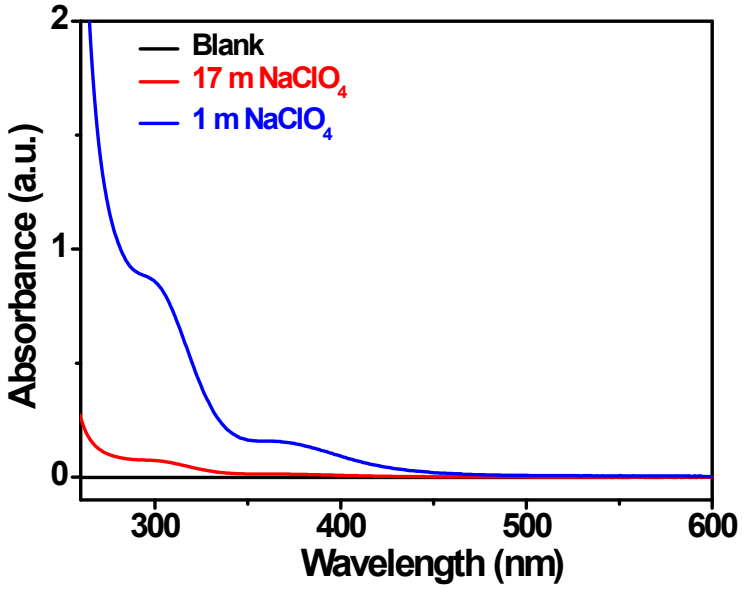

Fig. S26 UV-vis spectra of the various electrolyte after the stability studies.

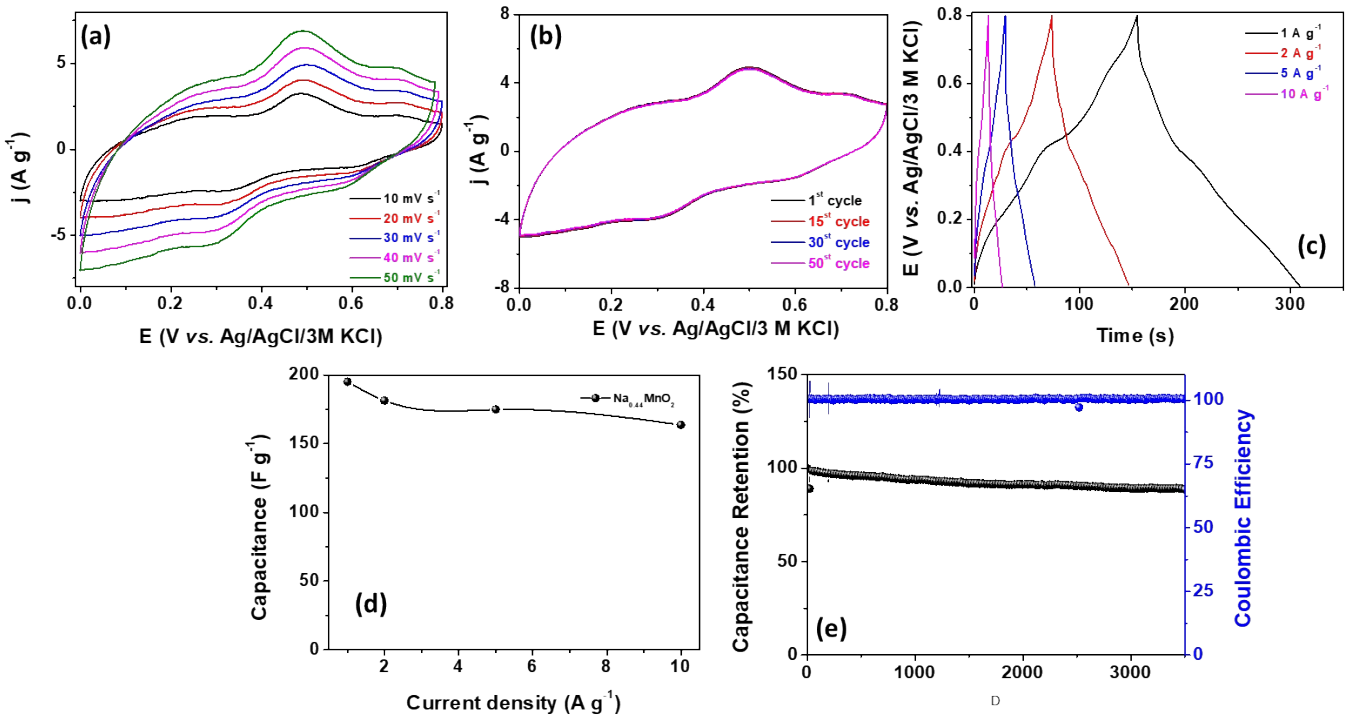

Fig. S27. (a) CVs of $Na_{0.44}MnO_2$ at various scan rates, (b) cycling stability at 30 mV s^{-1} (c) GCD curve of $Na_{0.44}MnO_2$ at various current densities, (d) corresponding capacitance *vs.* current density (e) capacitance retention up to 3500 cycles in 17 m $NaClO_4$ CE: Pt wire, RE: Ag/AgCl/3 M KCl.

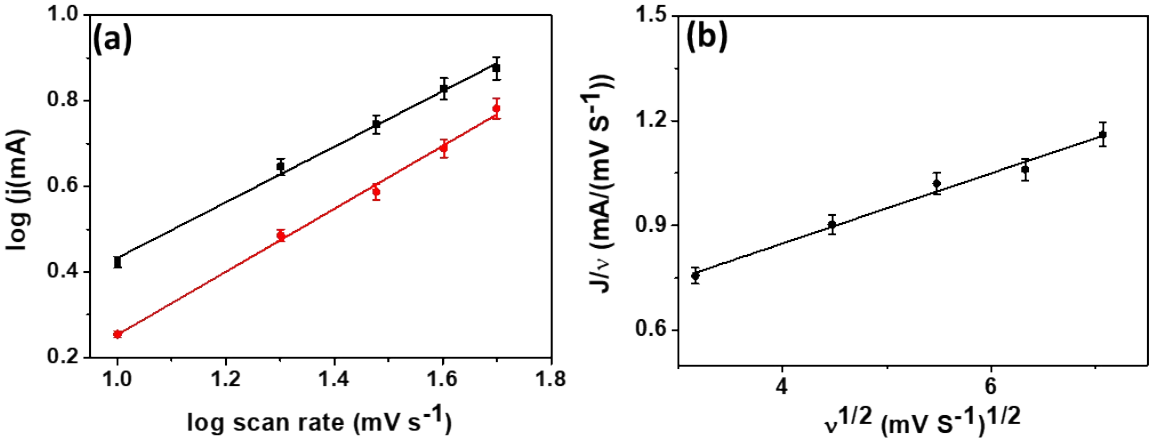

Fig. S28. (a) The logarithm plot of current density against logarithmic of scan rate to analyse b value,(b) plot of current per unit scan rate against the square root of scan rate in 17 m $NaClO_4$ CE: Pt wire, RE: Ag/AgCl/3 M KCl.

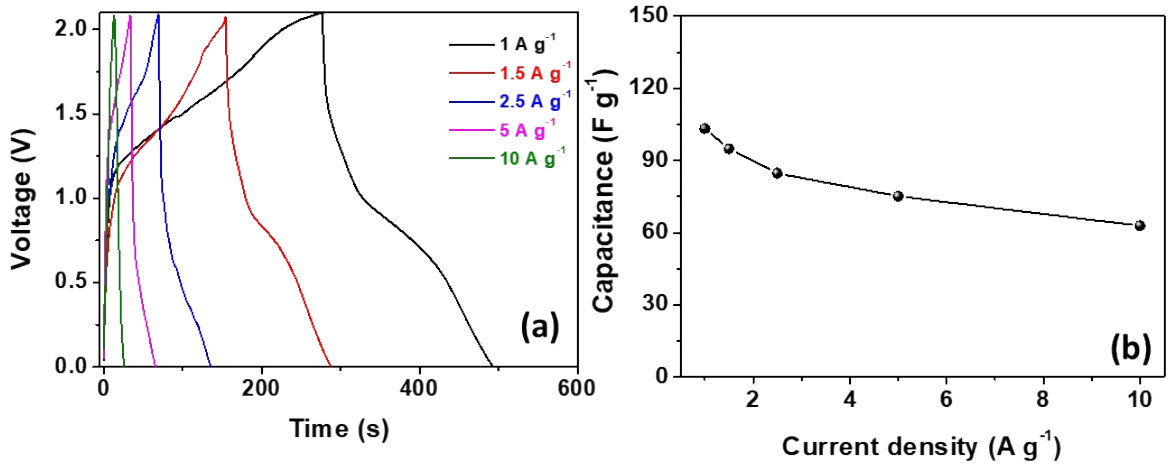

Fig. S29. GCD curves and, (b) capacitance for S@VC||$Na_{0.44}MnO_2$ in 17 m $NaClO_4$ at various scan current density.

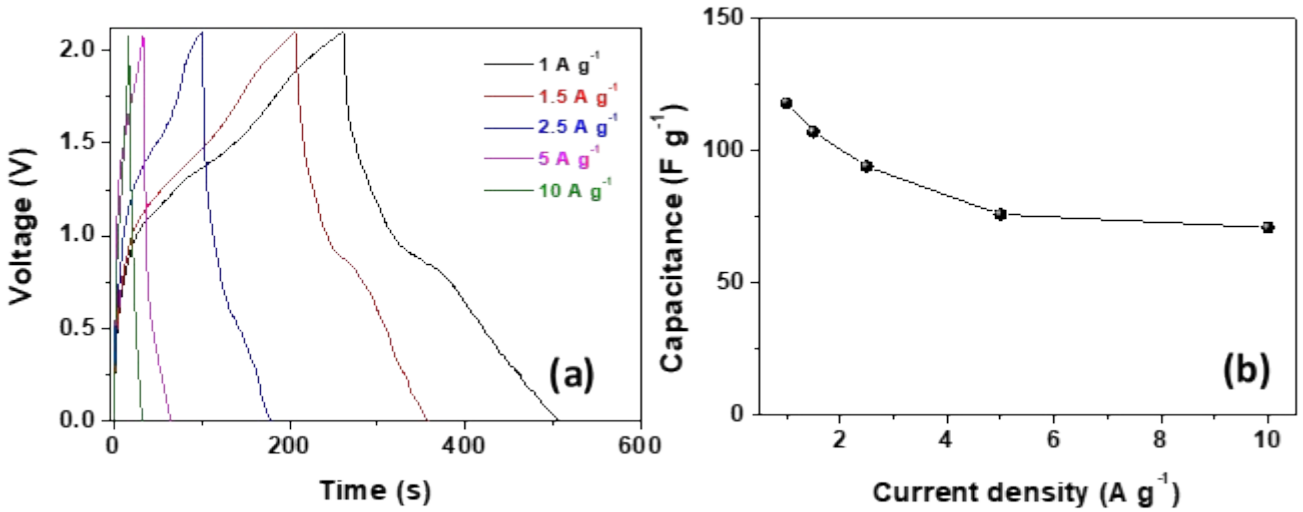

Fig. S30. GCD curves and, (b) capacitance for S@MNC-800||$Na_{0.44}MnO_2$ in 17 m $NaClO_4$ at various scan current density.

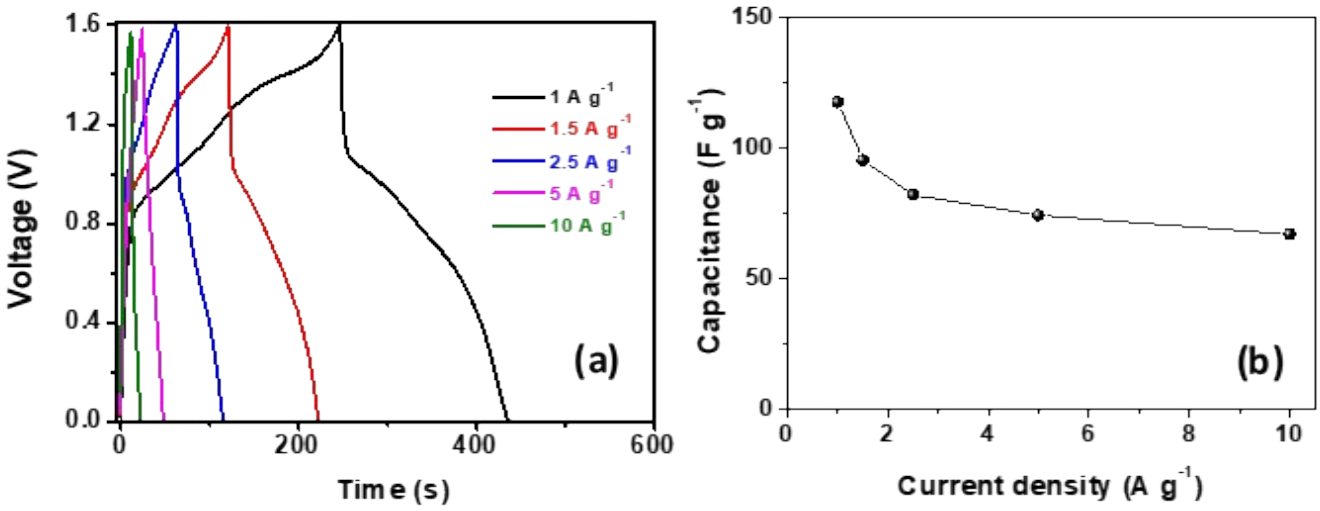

Fig. S31. (a) GCD curves of S@MNC-600||$Na_{0.44}MnO_2$ in 1 m $NaClO_4$ at various current densities, (b) are the corresponding capacitance *vs.* current density plot.

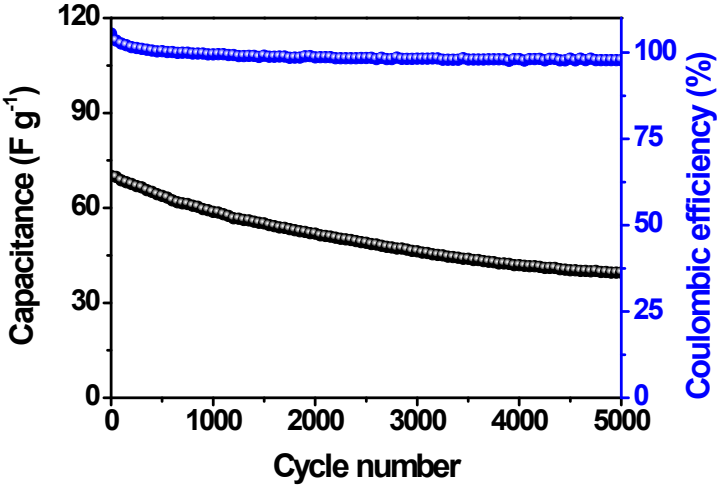

Fig. S32. cycling stability of S@MNC-600||$Na_{0.44}MnO_2$ in 1 m $NaClO_4$ up to 5000 cycles at 10 A g^{-1}.

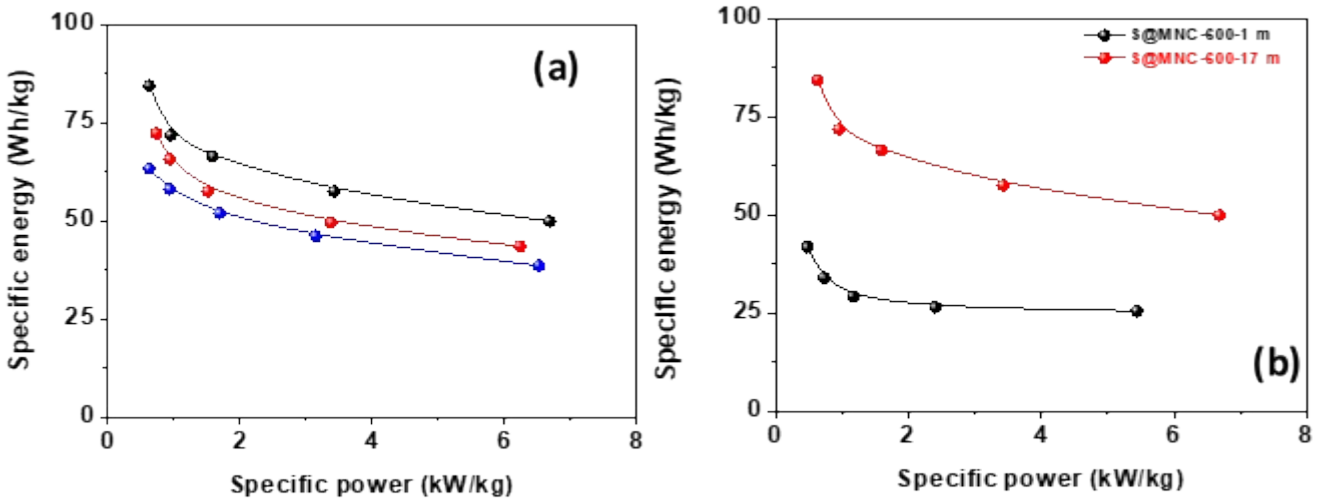

Fig. S33. Ragone plot showing energy density and power density of S@MNC-600||$Na_{0.44}MnO_2$ (black), S@MNC-800||$Na_{0.44}MnO_2$ (red), and S@VC||$Na_{0.44}MnO_2$ (blue), in (a) 17 m $NaClO_4$,(b) Ragone plot showing the comparison S@MNC-600||$Na_{0.44}MnO_2$ full cell in 17 m and 1 m $NaClO_4$.

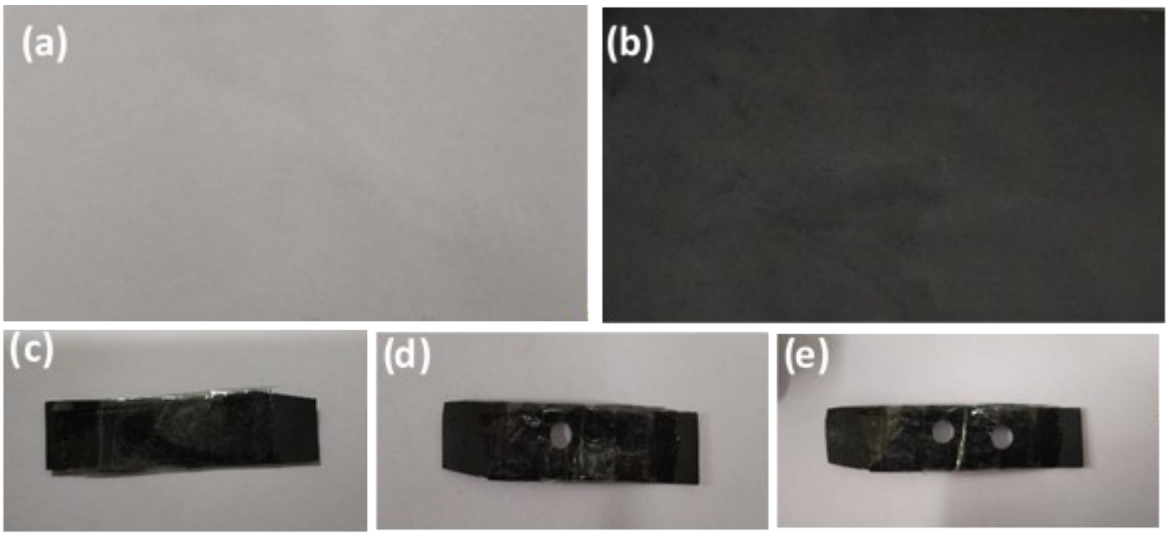

Fig. S34. Images of A4 size paper (a) before and (b) after carbon coating, (c) assembled hybrid Na-S full cell in (c) original state, (d) after punching a hole, and (e) after punching two holes.

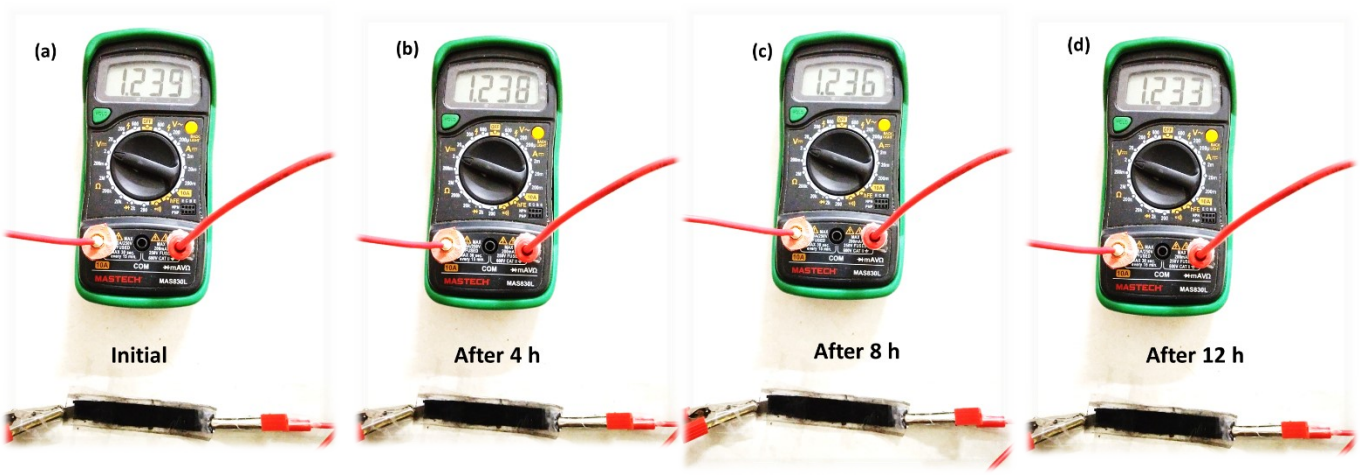

Fig. S35. Monitoring of OCP of a flexible paper-based Na-S hybrid full cell (a) initially, after (b) 4 h, (c) 8 h and 12 h.

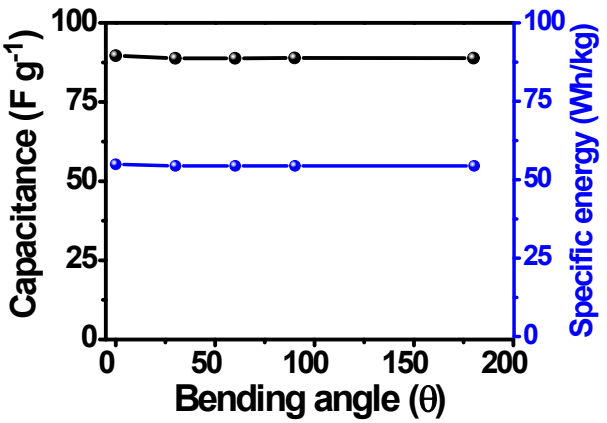

Fig. S36. Ragone plot showing energy and power density of S@MNC-600||$Na_{0.44}MnO_2$ in 17 m $NaClO_4$ at various deformations.

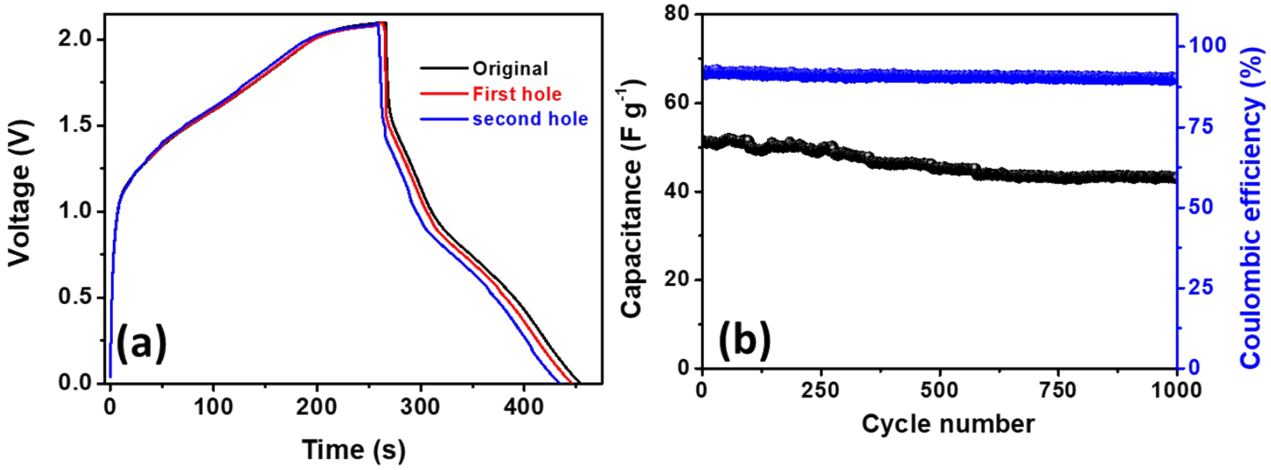

Fig. S37. (a) GCD curves for paper-based S@MNC-600||$Na_{0.44}MnO_2$ in 17 m $NaClO_4$ at various deformation state, (b) cycling stability at 8 A g^{-1} paper-based battery bended at an angle of 60 °.

References:

1. M. H. Lee, S. J. Kim, D. Chang, J. Kim, S. Moon, K. Oh, K.-Y. Park, W. M. Seong, H. Park and G. Kwon, *Mater. Today*, 2019, **29**, 26-36.